

1 **A SECOND-ORDER BOUND-PRESERVING EXPONENTIAL**  
2 **SCHEME FOR DEGENERATE PARABOLIC EQUATIONS \***

3 CHANG CHEN<sup>†</sup> AND CHI-WANG SHU<sup>‡</sup>

4 **Abstract.** This paper proposes a second-order numerical method for solving nonlinear parabolic  
5 equations with degenerate mobility. The intrinsic degenerate mobility in the equation yields a globally  
6 bounded solution. A pivotal feature of our methodology is an appropriate reformulation of the  
7 equation into an equivalent form. After applying a discontinuous Galerkin spatial discretization  
8 method, we derive a fully nonlinear ordinary differential equation (ODE) with a splitting structure.  
9 By introducing a linear term into the ODE, an exponential temporal discretization method, which  
10 involves only linear solvers, is proposed based on integrating factors and strong stability preserving  
11 (SSP) Runge-Kutta methods. Our approach is proven to exhibit second-order accuracy, ensures  
12 bound preservation and mass conservation, and demonstrates a favorable CFL condition  $\tau \sim h$ ,  
13 where  $\tau$  and  $h$  are the temporal and spatial mesh sizes respectively. Comprehensive numerical tests  
14 validate the second-order accuracy and bound-preserving behaviors of our method.

15 **Key words.** bound preservation, discontinuous Galerkin method, exponential scheme, SSP  
16 Runge-Kutta, degenerate parabolic equations

17 **MSC codes.** 65M12, 65M60, 35K65

18 **1. Introduction.** In this paper, we focus on designing numerical schemes for  
19 solving a class of degenerate parabolic equations of the form

20 (1.1) 
$$\begin{cases} \rho_t = \nabla f(\rho) \nabla (H'(\rho) + V(\mathbf{x}) + W * \rho), & \mathbf{x} \in \Omega, \quad t > 0, \\ \rho(\mathbf{x}, 0) = \rho_0(\mathbf{x}), & \mathbf{x} \in \Omega. \end{cases}$$

21 Here  $\Omega \subset \mathbb{R}^d$  with  $d = 1$  or  $2$ , and  $\rho(\mathbf{x}, t) : \Omega \times [0, +\infty) \rightarrow \mathbb{R}$  is the unknown particle  
22 density;  $f(\rho)$  is a nonlinear degenerate mobility function that may cause solutions  
23 to exhibit boundedness or non-smoothness; the  $H(\rho)$ ,  $V(\mathbf{x})$ , and  $W(\mathbf{x})$  are given  
24 functions with various meanings depending on the specific context [8, 30]. In this  
25 work, we assume that  $H(\rho)$  is convex and  $W(\mathbf{x}) = W(-\mathbf{x})$ . The equation (1.1) can  
26 be written as a gradient flow

27 
$$\rho_t = \nabla f(\rho) \nabla \left( \frac{\delta E(\rho)}{\delta \rho} \right)$$

28 with respect to the free energy functional

29 
$$E(\rho) = \int_{\Omega} H(\rho) + V\rho + \frac{1}{2}(W * \rho)\rho \, d\mathbf{x}.$$

30 The presence of the degenerate mobility  $f(\rho)$  introduces a complex layer of intri-  
31 cacy to the equation. Unlike its constant case, this type of mobility exerts a substantial  
32 influence over the global bound and continuity of solutions (see Section 4). Consider  
33 the mobility function  $f(\rho) = \rho(1 - \rho)$ . It remains positive within the interval  $(0,1)$   
34 and becomes degenerate at the endpoints 0 and 1. This characteristic ensures that

\*

**Funding:** The second author was supported by NSF grant DMS-2309249.

<sup>†</sup>Yau Mathematical Sciences Center, Tsinghua University, Beijing, 100084, China.  
(cc20@mails.tsinghua.edu.cn).

<sup>‡</sup>Division of Applied Mathematics, Brown University, Providence, RI 02912, USA. (chi-  
wang\_shu@brown.edu).

35 the solution to equation (1.1) with this specific mobility always stays confined within  
 36 the range  $[0, 1]$  (such as [16]). For our subsequent analysis, we make the assumption,  
 37 without loss of generality, that  $f(\rho) \geq 0$  for all  $\rho \in [0, 1]$  and the exact solution  $\rho$  of  
 38 equation (1.1) adheres to the condition that

$$39 \quad (1.2) \quad \rho(\mathbf{x}, t) \in [0, 1] \text{ for all } (\mathbf{x}, t) \in \Omega \times [0, +\infty).$$

40 Given this framework, the importance of a numerical scheme ensuring bound preser-  
 41 vation becomes evident when attempting to resolve (1.1).

42 There are extensive bound-preserving and high-order spatial numerical methods  
 43 for equation (1.1), such as the finite-difference method [26], finite-volume method [2,  
 44 3], discontinuous Galerkin method [23, 29] and references therein. For temporal dis-  
 45 cretization of (1.1), the implicit methods are commonly used to maintain stability and  
 46 preserve physical properties [2, 9, 27]. However, implicit bound-preserving schemes are  
 47 usually limited to first-order in time and necessitate the solution of a large non-linear  
 48 algebraic system at each time-step. Explicit temporal discretizations are computa-  
 49 tionally efficient at each iteration, but a parabolic CFL condition  $\tau \sim h^2$ , where  $\tau$  and  
 50  $h$  are temporal and spatial mesh sizes respectively, is normally required for explicit  
 51 schemes [29]. To strike a balance between efficiency and stability, implicit-explicit  
 52 (IMEX) methods are frequently utilized when the equation exhibits a splitting struc-  
 53 ture. The work [6] rewrote the model (1.1) as a splitting form

$$54 \quad (1.3) \quad \rho_t = \Delta\Phi(\rho) + \nabla f(\rho)\nabla(V(\mathbf{x}) + W * \rho) = \mathcal{C}(\rho) + \mathcal{D}(\rho)$$

55 with  $\Phi(\rho) = \int_0^\rho f(s)H''(s) ds$ , and they dealt implicitly with  $\mathcal{C}(\rho)$  and explicitly with  
 56  $\mathcal{D}(\rho)$  following the idea as in [5]. However, nonlinear systems were still required to be  
 57 solved using this splitting, and the preservation of positivity was only proven for the  
 58 first-order temporal scheme. This issue of limited accuracy is pervasive in the devel-  
 59 opment of bound-preserving schemes using classical IMEX-RK schemes, owing to the  
 60 infeasibility of implicit SSP-RK schemes with order higher than one [18]. Recently,  
 61 the IMEX-RK incorporating multi-derivatives [11, 17, 22] has offered the potential to  
 62 obtain high-order bound-preserving schemes. However, the assumption of high-order  
 63 derivatives is not easily applicable to the equation (1.1). Even if (1.1) is simplified  
 64 to the heat equation  $\rho = \Delta\rho$ , the second-order derivative  $\Delta^2$  no longer satisfies the  
 65 maximum bound principle. Furthermore, a variety of novel techniques have been de-  
 66 veloped for bound preservation, including Lagrange multiplier approaches [10, 31] and  
 67 the energy variational approach [14]. These approaches primarily confront challenges  
 68 in solving fully nonlinear implicit schemes or conducting rigorous error analysis for  
 69 general models.

70 An alternative prevalent way to explore high-order bound-preserving schemes is  
 71 by employing the exponential integrator (see [19] for a review). To the best of our  
 72 knowledge, no previous work has studied an exponential bound-preserving scheme for  
 73 (1.1), but numerous research studies have explored similar models from the insights  
 74 of exponential integrators. In contrast to (1.3), we reformulate (1.1) with a distinct  
 75 splitting structure

$$76 \quad (1.4) \quad \rho_t = \nabla F(\rho)\nabla\rho + \nabla f(\rho)\nabla(V(\mathbf{x}) + W * \rho) = \mathcal{L}(\rho)\rho + \mathcal{N}(\rho),$$

77 where  $F(\rho) = f(\rho)H''(\rho) \geq 0$ . By introducing a term  $L\rho$  as an approximation of  
 78  $\mathcal{L}(\rho)\rho$ , the equation (1.4) can be further written as

$$79 \quad (1.5) \quad \left( e^{\mathcal{T}(t)}\rho \right)_t = e^{\mathcal{T}(t)} ((\mathcal{L}(\rho) - L)\rho + \mathcal{N}(\rho)).$$

80 where  $\mathcal{T}(t) = \int_0^t L(s) ds$  is the integrating factor associated with  $L$ . The work [23]  
 81 took  $L = \mu I$  with a constant  $\mu > 0$ , which makes its computation similar to that of  
 82 explicit methods. However, their scheme required the parabolic CFL condition  $\tau \sim h^2$   
 83 analogous to explicit methods when attempting to apply it to our equation (1.4). In  
 84 cases where  $\mathcal{L}(\rho)$  is independent of  $\rho$ , several exponential linear schemes employing  
 85  $L = \mathcal{L}$  have been effectively utilized for (1.4) to generate bounded numerical solu-  
 86 tions [13, 24, 25]. In these works, the operator  $\mathcal{L}$  possesses a specific special structure,  
 87 resulting in a symmetry of either Toeplitz matrices or circulant matrices. Conse-  
 88 quently, FFT-based algorithms are adequate to achieve enhanced efficiency. Moreover,  
 89 the very recent study [7] also implemented a fixed constant approximation to  $\mathcal{L}$  that  
 90 depends only on the spatial vector  $\mathbf{x}$ , although the issue of bound-preservation has not  
 91 been addressed in their context. For  $\mathcal{L}(\rho)$  depending on  $\rho$ , the work [21] introduced  
 92 a second-order exponential scheme that incorporates  $L = \mathcal{L}(\rho)$ . This scheme needed  
 93 three to four evaluations of the fully nonlinear equation  $\rho_t = L(\rho)\rho$  per iteration.  
 94 When applied to our model (1.4), the computational burden generally resembles that  
 95 of implicit methods, despite their provision of detailed techniques for distinct stiff  
 96 kinetic equations.

97 Above all, it remains a significant challenge to compute a bound-preserving solu-  
 98 tion to (1.1) while achieving both high-order accuracy and efficiency. In this paper,  
 99 we adopt the splitting (1.4) and present a second-order scheme using an exponential  
 100 integrator associated with  $L = \mathcal{L}(\rho^*)$ , where  $\rho^*$  is explicitly given. At each itera-  
 101 tion, our scheme only requires three times of computation for the linear equation  
 102  $\rho = L(\rho^*)\rho$ , which can be efficiently evaluated by numerous existing algorithms (see  
 103 the review [28]). As evidenced in prior studies, the Krylov- or Leja-based method-  
 104 ologies often surpass implicit schemes in many practical applications [12, 15]. Import-  
 105 antly, we demonstrate that our method is mass-conservative, bound-preserving and  
 106 benefits from a favorable CFL condition  $\tau \sim h$ .

107 **2. Spatial discretization.** In this section, we present a spatial discretization  
 108 method for parabolic equations (1.1) using a discontinuous Galerkin (DG) approach.  
 109 We only consider the one-dimensional case ( $d = 1$ ) as an demonstration and the two-  
 110 dimensional case ( $d = 2$ ) can be derived in the same way (see [29, Section 3]). In our  
 111 following statement, we denote  $x = \mathbf{x}$  as a spatial variable in one-dimensional space.

112 Let  $I_i = (x_{i-\frac{1}{2}}, x_{i+\frac{1}{2}})$  and  $I = \cup_{i=1}^N I_i$  be a partition of the domain  $\Omega$ . For  
 113 simplicity, we consider uniform meshes  $h = x_{i+\frac{1}{2}} - x_{i-\frac{1}{2}}$ , but this assumption is not  
 114 essential. The discontinuous piecewise polynomial space is defined as

$$115 \quad V_h = \{v_h : v_h|_{I_i} \in P^k(I_i), i = 1, 2, \dots, N\},$$

116 where  $P^k(I_i)$  is the space of  $k$ -th order polynomial. We use the notation  $v_h^+$  and  $v_h^-$  as  
 117 the right and left limit of  $v_h \in V_h$  respectively. For a function  $s = s(\rho)$  or  $s = s(\rho, x)$ ,  
 118 we denote by  $s_h = s(\rho_h)$  or  $s_h = s(\rho_h, x)$  respectively. Furthermore, the notation  $s_h^+$   
 119 stands for  $s(\rho_h^+)$  or  $s(\rho_h^+, x)$ , and  $s_h^-$  stands for  $s(\rho_h^-)$  or  $s(\rho_h^-, x)$ . For the purpose of  
 120 this paper, we only consider the second-order DG scheme ( $k = 1$ ) and choose

$$121 \quad (2.1) \quad \phi_i^{(1)} = \frac{x_{i+\frac{1}{2}} - x}{h}, \quad \phi_i^{(2)} = \frac{x - x_{i-\frac{1}{2}}}{h},$$

as the basis for  $P^1(I_i)$ . Note that  $x_{i\pm\frac{1}{2}}$  are the  $k+1$  Gauss-Lobatto quadrature points

on  $I_i$  when  $k = 1$ . The Gauss-Lobatto quadrature on  $x_{i\pm\frac{1}{2}}$  can be defined by

$$\widetilde{\int}_{I_i} \eta \zeta \, dx = \frac{h}{2} \left( (\eta \zeta)_{i-\frac{1}{2}}^+ + (\eta \zeta)_{i+\frac{1}{2}}^- \right)$$

and

$$\widetilde{\int}_{I_i} \eta \partial_x \zeta \, dx = \frac{h}{2} \left( (\eta \partial_x (\mathcal{I} \zeta))_{i-\frac{1}{2}}^+ + (\eta \partial_x (\mathcal{I} \zeta))_{i+\frac{1}{2}}^- \right),$$

122 where the operator  $\mathcal{I}$  returns the first-order polynomial interpolating at  $x_{i\pm\frac{1}{2}}$ . As a  
123 convention,  $\widetilde{\int}_{\Omega}$  stands for  $\sum_i \widetilde{\int}_{I_i}$ .

124 To define the DG method, we first introduce auxiliary variables to split the original  
125 problem (1.4) into the following system of first-order equations:

$$\begin{aligned} \rho_t &= \partial_x (F(\rho)\eta) + \partial_x (f(\rho)u), \\ \eta &= \partial_x \rho, \\ u &= \partial_x \xi, \\ \xi &= V(x) + W * \rho. \end{aligned}$$

127 A periodic or compactly supported boundary condition is considered in this work,  
128 but our work can extend to more general types of boundary conditions, such as zero-  
129 flux boundary conditions. Then our DG approximation can be described as: Find  
130  $\rho_h, \eta_h, u_h, \xi_h \in V_h$  such that for any  $\phi_h, \psi_h, \varphi_h \in V_h$ ,

$$\begin{aligned} (2.2) \quad \widetilde{\int}_{I_i} (\rho_h)_t \phi_h \, dx &= - \widetilde{\int}_{I_i} (F_h \eta_h) \partial_x \phi_h \, dx + (\widehat{F_h \eta_h})_{i+\frac{1}{2}} (\phi_h)_{i+\frac{1}{2}}^- - (\widehat{F_h \eta_h})_{i-\frac{1}{2}} (\phi_h)_{i-\frac{1}{2}}^+ \\ &\quad - \widetilde{\int}_{I_i} (f_h u_h) \partial_x \phi_h \, dx + (\widehat{f_h u_h})_{i+\frac{1}{2}} (\phi_h)_{i+\frac{1}{2}}^- - (\widehat{f_h u_h})_{i-\frac{1}{2}} (\phi_h)_{i-\frac{1}{2}}^+ \\ 131 \quad \widetilde{\int}_{I_i} \eta_h \psi_h \, dx &= - \widetilde{\int}_{I_i} \rho_h \partial_x \psi_h \, dx + (\widehat{\rho_h})_{i+\frac{1}{2}} (\psi_h)_{i+\frac{1}{2}}^- - (\widehat{\rho_h})_{i-\frac{1}{2}} (\psi_h)_{i-\frac{1}{2}}^+ \\ \widetilde{\int}_{I_i} u_h \varphi_h \, dx &= - \widetilde{\int}_{I_i} \xi_h \partial_x \varphi_h \, dx + (\widehat{\xi_h})_{i+\frac{1}{2}} (\varphi_h)_{i+\frac{1}{2}}^- - (\widehat{\xi_h})_{i-\frac{1}{2}} (\varphi_h)_{i-\frac{1}{2}}^+ \\ &\quad (\xi_h)_i = V(x_i) + (W * \rho_h)(x_i) \end{aligned}$$

132 When  $W$  is smooth, the convolution can be approximated by

$$133 \quad (W * \rho_h)(x_i) \approx \widetilde{\int}_{\Omega} W(x_i - y) \rho_h(y) \, dy.$$

134 The numerical fluxes are chosen in the following way

$$135 \quad (2.3a) \quad \widehat{F_h \eta_h} = (F_h \eta_h)^+, \widehat{\rho_h} = \rho_h^- \quad \text{or} \quad \widehat{F_h \eta_h} = (F_h \eta_h)^-, \widehat{\rho_h} = \rho_h^+,$$

$$136 \quad (2.3b) \quad \widehat{f_h u_h} = \frac{1}{2} \left( (f_h u_h)^+ + (f_h u_h)^- + \alpha (g^+ - g^-) \right), \quad \alpha = \max\{|u_h|^+, |u_h|^-\},$$

$$137 \quad (2.3c) \quad \xi_h = \frac{1}{2} (\xi_h^+ + \xi_h^-),$$

139 where  $g$  is chosen to satisfy  $\text{sign}[g_h] = \text{sign}[f_h]$  or  $\text{sign}[g_h] = 0$ , and  $\alpha g \pm f u \in [0, \alpha]$   
140 when all  $\rho \in [0, 1]$ . For the case  $f = \rho(1 - \rho)$ , we can take  $g = \rho$ . Using the fact  
141  $\alpha \geq |u|$ , it is straightforward to confirm that  $\alpha g \pm f u \in [0, \alpha]$  for  $\rho \in [0, 1]$ .

142 *Remark 2.1.* If only positivity preservation is required,  $g$  in (2.3) can be relaxed  
143 to satisfy  $\alpha g \pm fu \geq 0$  as suggested by [29].

144 Subsequently, we reformulate (2.2) into a vector ODE corresponding to the values  
145 on all Gauss-Lobatto nodes. Let

$$146 \quad (2.4) \quad \rho_h(x, t) = \rho_i^{(1)}(t)\phi_i^{(1)}(x) + \rho_i^{(2)}(t)\phi_i^{(2)}(x), \quad x \in I_i, \quad t \geq 0,$$

147 where  $\phi_i^{(1)}, \phi_i^{(2)}$  are given in (2.1). Define  $\boldsymbol{\rho}_h(t) = (\rho_1^{(1)}(t), \rho_1^{(2)}(t), \dots, \rho_N^{(1)}(t), \rho_N^{(2)}(t))^\top$   
148 as the vector representing the values of  $\rho_h$  on all Gauss-Lobatto nodes. By employing  
149 the basis functions  $\phi_i^{(1)}$  and  $\phi_i^{(2)}$  in the DG discretization (2.2), we can derive an ODE  
150 of the following form:

$$151 \quad (2.5) \quad (\boldsymbol{\rho}_h)_t = \mathcal{L}_h(\boldsymbol{\rho}_h)\boldsymbol{\rho}_h + \mathcal{N}_h(\boldsymbol{\rho}_h),$$

152 where  $\mathcal{L}_h(\boldsymbol{\rho}_h) \in \mathbb{R}^{2N \times 2N}$  is a matrix linked to the discretization of  $\partial_x F(\rho)\nabla$ , and  
153  $\mathcal{N}_h(\boldsymbol{\rho}) \in \mathbb{R}^{2N}$  is a vector associated with the discretization of  $\partial_x(f(\rho)u)$ . Employing  
154 the flux (2.3a) along with periodic boundary conditions, two asymmetric operator  
155  $\mathcal{L}_h(\boldsymbol{\rho})$  are obtained with off-diagonal elements involving difference  $F(\rho_i^{(1)}) - F(\rho_i^{(2)})$  or  
156  $F(\rho_i^{(2)}) - F(\rho_i^{(1)})$ , which can be negative. In this work, we average the two asymmetric  
157 operators to obtain a symmetric one

$$158 \quad (2.6) \quad \mathcal{L}_h(\boldsymbol{\rho}_h) = \frac{1}{h^2} \begin{pmatrix} d_1^1 & 0 & F_1^2 & & & & & & & F_N^2 & a_1 \\ 0 & d_1^2 & a_2 & F_2^1 & & & & & & & F_1^1 \\ F_1^2 & a_2 & d_2^1 & 0 & F_2^2 & & & & & & \\ & F_2^1 & 0 & d_2^2 & a_3 & F_3^1 & & & & & \\ & & \ddots & \ddots & \ddots & \ddots & \ddots & & & & \\ & & & F_{i-1}^2 & a_i & d_i^1 & 0 & F_i^2 & & & \\ & & & & F_i^1 & 0 & d_i^2 & a_{i+1} & F_{i+1}^1 & & \\ & & & & & \ddots & \ddots & \ddots & \ddots & & \\ F_N^2 & & & & & & F_{N-1}^2 & a_{N-1} & d_N^1 & 0 & \\ a_1 & F_1^1 & & & & & & F_N^1 & 0 & d_N^2 & \end{pmatrix}_{2N \times 2N}$$

159 where  $F_i^\ell = F(\rho_i^{(\ell)})$  and

$$160 \quad d_i^1 = -(F_i^2 + F_i^1 + 2F_{i-1}^2), \quad d_i^2 = -(2F_{i+1}^1 + F_i^2 + F_i^1), \quad a_i = F_i^1 + F_{i-1}^2.$$

162 Consequently, using the fact  $F = fH'' \geq 0$ , one obtains that  $\mathcal{L}_h(\boldsymbol{\rho}_h) = (\ell_{ij})_{2N \times 2N}$  is  
163 symmetric and has the following properties:

- 164 • Zero row sums:  $\mathcal{L}_h(\boldsymbol{\rho}_h)\mathbf{1} = 0$  with  $\mathbf{1} = (1, 1, \dots, 1)^\top \in \mathbb{R}^{2N}$ .
- 165 • Pattern of signs:  $\ell_{ij} \geq 0$  if  $i = j$ , and  $\ell_{ij} \leq 0$  if  $i \neq j$ .

166 Matrices exhibiting both of these characteristics are known as graph Laplacians [4],  
167 which lead to an ODE that guarantees both mass conservation and bound preserva-  
168 tion. For a vector  $\boldsymbol{\rho}$ , we denote  $\boldsymbol{\rho} \in [0, 1]$  or  $0 \leq \boldsymbol{\rho} \leq 1$  to indicate that every element  
169 of  $\boldsymbol{\rho}$  falls within the range of 0 to 1. Based on this notation, we present the following  
170 classical conclusion:

171 **LEMMA 2.2** ([4, Proposition 1.1]). *Let the matrix  $\mathcal{L}_h(\boldsymbol{\rho}_h)$  be defined as (2.6) and*  
172  *$\mathbf{u}(t)$  be a solution to the ODE*

$$173 \quad (2.7) \quad \mathbf{u}_t = \mathcal{L}_h(\boldsymbol{\rho}_h)\mathbf{u}, \quad \mathbf{u}(0) = \mathbf{u}_0$$

174 *with  $\mathbf{u}_0 \in [0, 1]$ . Then for all  $t \geq 0$ ,  $\mathbf{u}(t) \in [0, 1]$  and  $\mathbf{1}^\top \mathbf{u}(t) = \mathbf{1}^\top \mathbf{u}_0$ .*

175 Alternatively, we can express the solution of the ODE (2.7) using an exponential  
176 matrix as

$$177 \quad \mathbf{u}(t) = e^{t\mathcal{L}_h(\boldsymbol{\rho}_h)} \mathbf{u}_0.$$

178 Therefore, Lemma 2.2 demonstrates that the exponential matrix  $e^{t\mathcal{L}_h(\boldsymbol{\rho}_h)}$  ensures both  
179 mass conservation and bound preservation.

180 **3. Temporal discretization.** In this section, we present first- and second-order  
181 bound-preserving temporal discretizations for the ODE (2.5). Our schemes are de-  
182 signed by incorporating an auxiliary linear term independent of  $\boldsymbol{\rho}_h$  and then employ-  
183 ing an exponential integrator. For simplicity, the time domain is discretized using  
184 equispaced points with time-stepping  $\tau > 0$ , and we define the  $n$ th point given by  
185  $t_n = n\tau$  ( $n = 0, 1, 2, \dots$ ). Considering the ODE (2.5) on the interval  $[t_n, t_{n+1}]$ , we  
186 reformulate it as

$$187 \quad (3.1) \quad (\boldsymbol{\rho}_h)_t = L_p(t)\boldsymbol{\rho}_h + \mathcal{N}_h(\boldsymbol{\rho}_h) + (\mathcal{L}_h(\boldsymbol{\rho}_h) - L_p(t))\boldsymbol{\rho}_h, \quad (x, t) \in \Omega \times [t_n, t_{n+1}],$$

188 where  $L_p(t)$  is a  $p$ th-order approximation of  $\mathcal{L}_h(\boldsymbol{\rho}_h(t))$  satisfying

$$189 \quad (3.2) \quad \mathcal{L}_h(\boldsymbol{\rho}_h(t_n + s)) = L_p(t_n + s) + O(s^p), \quad s \in [0, \tau].$$

190 Define the integrating factor

$$191 \quad (3.3) \quad \mathcal{T}(t) = \int_0^t L_p(s) ds.$$

192 Then, the equation (3.1) can be written as

$$193 \quad (3.4) \quad \left( e^{-\mathcal{T}(t)} \boldsymbol{\rho}_h(t) \right)_t = e^{-\mathcal{T}(t)} (\mathcal{N}_h(\boldsymbol{\rho}_h(t)) + (\mathcal{L}_h(\boldsymbol{\rho}_h(t)) - L_p(t))\boldsymbol{\rho}_h(t))$$

194 Define  $\mathbf{w}(t) = e^{-\mathcal{T}(t)} \boldsymbol{\rho}_h(t)$ . We get

$$195 \quad (3.5) \quad (\mathbf{w}(t))_t = e^{-\mathcal{T}(t)} (\mathcal{N}_h(\boldsymbol{\rho}_h(t)) + (\mathcal{L}_h(\boldsymbol{\rho}_h(t)) - L_p(t))\boldsymbol{\rho}_h(t)) = H(\mathbf{w}, t).$$

196 Next, we introduce first- and second-order bound-preserving schemes for (3.5) using  
197 SSP-RK methods [18]. It is noteworthy that our proposed schemes are simplified to  
198 the exponential SSP-RK methods [24] when  $\mathcal{L}_h(\boldsymbol{\rho}_h)$  is a constant matrix independent  
199 of  $\boldsymbol{\rho}_h$ .

200 **3.1. First-order scheme.** Consider the approximation  $L_0(t) = \mathcal{L}_h(\boldsymbol{\rho}_h(t_n))$ .  
201 Then the integrating factor (3.3) becomes  $\mathcal{T}(t) = t\mathcal{L}_h(\boldsymbol{\rho}_h(t_n))$ . By applying the  
202 first-order forward Euler scheme to (3.5), we derive the scheme

$$203 \quad (3.6) \quad \boldsymbol{\rho}_h^{n+1} = e^{\tau\mathcal{L}_h(\boldsymbol{\rho}_h^n)} (\boldsymbol{\rho}_h^n + \tau\mathcal{N}_h(\boldsymbol{\rho}_h^n)),$$

204 which is equivalent to

$$205 \quad (3.7a) \quad \boldsymbol{\rho}_h^{n+1,1} = \boldsymbol{\rho}_h^n + \tau\mathcal{N}_h(\boldsymbol{\rho}_h^n)$$

$$206 \quad (3.7b) \quad \boldsymbol{\rho}_h^{n+1} = e^{\tau\mathcal{L}_h(\boldsymbol{\rho}_h^n)} \boldsymbol{\rho}_h^{n+1,1}.$$

208 Let  $\rho_h(t)$  be an exact solution of (2.5) and denote  $\rho = \rho_h(t_n)$ . Using Taylor's expansion,  
 209 we have

$$\begin{aligned} \rho_h(t_{n+1}) - \rho_h^{n+1} &= \rho_h(t_{n+1}) - e^{\tau \mathcal{L}_h(\rho)} (\rho + \tau \mathcal{N}_h(\rho)) \\ &= \rho_h(t_{n+1}) - (I + \tau \mathcal{L}_h(\rho) + O(\tau^2)) (\rho + \tau \mathcal{N}_h(\rho)) \\ &= \rho_h(t_{n+1}) - (\rho + \tau (\mathcal{L}_h(\rho)\rho + \mathcal{N}_h(\rho))) + O(\tau^2) \\ &= O(\tau^2). \end{aligned}$$

211 Hence, the scheme (3.7) is a first-order temporal discretization for (2.5).

212 Alternatively, we can express the scheme (3.7) in a weak form: Find  $\rho_h^{n+1,1}, \rho_h^{n+1} \in$   
 213  $V_h$  such that for all  $\phi_h, \psi_h \in V_h$ ,

(3.8a)

$$\int_{I_i} \frac{\rho_h^{n+1,1} - \rho_h^n}{\tau} \phi_h \, dx = - \int_{I_i} (f_h^n u_h^n) \partial_x \phi_h \, dx + (\widehat{f_h^n u_h^n})_{i+\frac{1}{2}} (\phi_h)_{i+\frac{1}{2}}^- - (\widehat{f_h^n u_h^n})_{i-\frac{1}{2}} (\phi_h)_{i-\frac{1}{2}}^+,$$

(3.8b)

$$\int_{I_i} u_h^n \varphi_h \, dx = - \int_{I_i} \xi_h^n \partial_x \varphi_h \, dx + (\widehat{\xi_h^n})_{i+\frac{1}{2}} (\varphi_h)_{i+\frac{1}{2}}^- - (\widehat{\xi_h^n})_{i-\frac{1}{2}} (\varphi_h)_{i-\frac{1}{2}}^+,$$

$$(3.8c) \quad (\xi_h^n)_i = V(x_i) + (W * \rho_h^n)(x_i),$$

218 and  $\rho_h^{n+1} = (\tilde{\rho}_h^L(\tau) + \tilde{\rho}_h^R(\tau))/2$  with  $\tilde{\rho}_h : [0, \tau] \rightarrow V_h$  solving the system

$$(3.9a) \quad \int_{I_i} (\tilde{\rho}_h)_t \phi_h \, dx = - \int_{I_i} (F_h^n \eta_h) \partial_x \phi \, dx + (\widehat{F_h^n \eta_h})_{i+\frac{1}{2}} \phi_{i+\frac{1}{2}}^- - (\widehat{F_h^n \eta_h})_{i-\frac{1}{2}} \phi_{i-\frac{1}{2}}^+,$$

$$(3.9b) \quad \int_{I_i} \eta_h \psi_h \, dx = - \int_{I_i} \tilde{\rho}_h \partial_x \psi_h \, dx + (\widehat{\tilde{\rho}_h})_{i+\frac{1}{2}} (\psi_h)_{i+\frac{1}{2}}^- - (\widehat{\tilde{\rho}_h})_{i-\frac{1}{2}} (\psi_h)_{i-\frac{1}{2}}^+,$$

$$(3.9c) \quad \tilde{\rho}_h(0) = \rho_h^{n+1,1}.$$

223 and  $\tilde{\rho}_h^L, \tilde{\rho}_h^R$  correspond to the solutions using two different fluxes according to (2.3a).

224 LEMMA 3.1. Given  $\rho_h^n$ , the  $\rho_h^{n+1,1}$  solved in (3.8) satisfies

- 225 • Mass conservation:  $\int_{\Omega} \rho_h^{n+1,1} \, dx = \int_{\Omega} \rho_h^n \, dx$ ;
- 226 • Bound-preservation for the cell average: Assuming that  $\rho_h^n$  is within the  
 227 range  $[0, 1]$  at the Gauss-Lobatto quadrature, i.e.,  $\rho_h^n \in [0, 1]$ , the cell average  
 228  $(\bar{\rho}_h)_i^{n+1,1} = \frac{1}{h} \int_{I_i} \rho_h^{n+1,1} \, dx \in [0, 1]$  if

$$(3.10) \quad \alpha \lambda g \leq \rho \text{ and } \alpha \lambda (1 - g) \leq 1 - \rho,$$

230 where  $\lambda = \tau/h$ . Specifically, when  $g = \rho$ , it reduces to the CFL condition

$$(3.11) \quad \tau \leq \frac{h}{\max_{i=1, \dots, N} \alpha_{i \pm \frac{1}{2}}}.$$

232 *Proof.* Let  $\phi_h \equiv 1$  in (3.8a), we obtain that

$$(3.12) \quad \int_{I_i} \rho_h^{n+1,1} \, dx = \int_{I_i} \rho_h^n \, dx + \tau \left( (\widehat{f_h^n u_h^n})_{i+\frac{1}{2}} - (\widehat{f_h^n u_h^n})_{i-\frac{1}{2}} \right), \quad i = 1, 2, \dots, N.$$

234 Summing  $i$  from 1 to  $N$ , one get

$$235 \quad \widetilde{\int}_{\Omega} \rho_h^{n+1,1} dx = \widetilde{\int}_{\Omega} \rho_h^n dx + \tau \left( (\widehat{f_h^n u_h^n})_{N+\frac{1}{2}} - (\widehat{f_h^n u_h^n})_{-\frac{1}{2}} \right).$$

236 The numerical flux at the right boundary is equal to the numerical flux at the left  
237 boundary, as required by the periodic boundary condition and the definition of the  
238 numerical flux. Therefore, we can conclude that  $\widetilde{\int}_I \rho_h^{n+1,1} dx = \widetilde{\int}_I \rho_h^n dx$ .

239 Multiplying both side of (3.12) with  $1/h$ , it becomes

$$240 \quad (\bar{\rho}_h)_i^{n+1,1} = (\bar{\rho}_h)_i^n + \lambda \left( (\widehat{f_h^n u_h^n})_{i+\frac{1}{2}} - (\widehat{f_h^n u_h^n})_{i-\frac{1}{2}} \right), \quad i = 1, 2, \dots, N.$$

241 Note that the Gauss–Lobatto quadrature is exact for evaluating the cell average  $(\bar{\rho}_h)_i^n$   
242 since  $(\rho_h)_i^n$  is a first-order polynomial. For simplicity, we omit the indices  $n$  and  $h$  for  
243 the notation  $\rho_h^n$  in the subsequent proof. Then

$$\begin{aligned} (\bar{\rho})_i^{n+1,1} &= \frac{1}{2} \left( \rho_{i+\frac{1}{2}}^- + \rho_{i-\frac{1}{2}}^+ \right) + \frac{\lambda}{2} \left( (fu)_{i+\frac{1}{2}}^+ + (fu)_{i+\frac{1}{2}}^- + \alpha_{i+\frac{1}{2}} (g_{i+\frac{1}{2}}^+ - g_{i+\frac{1}{2}}^-) \right) \\ &\quad - \frac{\lambda}{2} \left( (fu)_{i-\frac{1}{2}}^+ + (fu)_{i-\frac{1}{2}}^- + \alpha_{i-\frac{1}{2}} (g_{i-\frac{1}{2}}^+ - g_{i-\frac{1}{2}}^-) \right) \\ &= \frac{1}{2} \left[ \rho_{i+\frac{1}{2}}^- + \lambda \left( (fu)_{i+\frac{1}{2}}^+ + (fu)_{i+\frac{1}{2}}^- + \alpha_{i+\frac{1}{2}} (g_{i+\frac{1}{2}}^+ - g_{i+\frac{1}{2}}^-) \right) \right. \\ &\quad \left. - \lambda \left( (fu)_{i+\frac{1}{2}}^- + (fu)_{i-\frac{1}{2}}^+ + \alpha_{i+\frac{1}{2}} (g_{i+\frac{1}{2}}^- - g_{i-\frac{1}{2}}^+) \right) \right] + \\ &\quad \frac{1}{2} \left[ \rho_{i-\frac{1}{2}}^+ + \lambda \left( (fu)_{i+\frac{1}{2}}^- + (fu)_{i-\frac{1}{2}}^+ + \alpha_{i+\frac{1}{2}} (g_{i+\frac{1}{2}}^- - g_{i-\frac{1}{2}}^+) \right) \right. \\ 244 \quad &\quad \left. - \lambda \left( (fu)_{i-\frac{1}{2}}^+ + (fu)_{i-\frac{1}{2}}^- + \alpha_{i-\frac{1}{2}} (g_{i-\frac{1}{2}}^+ - g_{i-\frac{1}{2}}^-) \right) \right] \\ &= \frac{1}{2} \left[ \lambda \alpha_{i+\frac{1}{2}} K^+(\rho_{i+\frac{1}{2}}^+, \alpha_{i+\frac{1}{2}}) + \lambda \alpha_{i+\frac{1}{2}} K^-(\rho_{i-\frac{1}{2}}^+, \alpha_{i+\frac{1}{2}}) \right. \\ &\quad \left. + \left( \rho_{i+\frac{1}{2}}^- - 2\lambda \alpha_{i+\frac{1}{2}} g_{i+\frac{1}{2}}^- \right) \right] \\ &\quad \frac{1}{2} \left[ \lambda \alpha_{i-\frac{1}{2}} K^-(\rho_{i-\frac{1}{2}}^-, \alpha_{i-\frac{1}{2}}) + \lambda \alpha_{i+\frac{1}{2}} K^+(\rho_{i+\frac{1}{2}}^-, \alpha_{i+\frac{1}{2}}) \right. \\ &\quad \left. + \left( \rho_{i-\frac{1}{2}}^+ - \lambda (\alpha_{i+\frac{1}{2}} + \alpha_{i-\frac{1}{2}}) g_{i-\frac{1}{2}}^+ \right) \right], \end{aligned}$$

245 where  $K^\pm = g \pm fu/\alpha$ . Note that  $K^\pm \in [0, 1]$  by the choice of  $g$ . To make  $(\bar{\rho}_h)_i^{n+1,1} \in$   
246  $[0, 1]$ , it is sufficient to ensure  $\rho - \lambda \alpha g \in [0, 1 - \lambda \alpha]$ , which reduces to the restriction  
247 (3.10).  $\square$

248 *Remark 3.2.* In the definition of  $\xi_h$ , it is continuous and (3.8b) gives  $u_h = \partial_x \mathcal{I}(\xi_h)$   
249 on  $I_i$  after integration by parts. Hence the CFL condition (3.11) becomes

$$250 \quad \tau \leq \frac{h}{\max_i \|\partial_x \mathcal{I}(\xi_h)\|_{L^\infty(I_i)}} \sim h,$$

251 which is a favorable CFL condition for parabolic equations.

252 *Remark 3.3.* For efficient implementation, we can approximate the exponential  
253 matrix in (3.7b) as

$$254 \quad (3.13) \quad \rho_h^{n+1} = (I - \tau \mathcal{L}_h(\rho_h^n))^{-1} \rho_h^{n+1,1},$$



255 which is also a first-order scheme [5] and the bound preservation still holds using the  
256 similar proving process.

257 As stated in Lemma 3.1, the Euler forward stage (3.7a) only maintains bound-  
258 preservation on the cell average, not across all Gauss-Lobatto quadrature points.  
259 Following the methodology developed by [32], we can apply a bound-preserving limiter  
260 to enforce the boundedness of nodal values on all Gauss-Lobatto quadrature points  
261 without violating the mass conservation and accuracy. Precisely, let

$$262 \quad \rho_h^{n+1,2}(x_{i\pm\frac{1}{2}}^\mp) = (\bar{\rho}_h)_i^{n+1,1} + \theta_i \left( \rho_h^{n+1,1}(x_{i\pm\frac{1}{2}}^\mp) - (\bar{\rho}_h)_i^{n+1,1} \right),$$

263 with

$$264 \quad \theta_i = \min \left\{ \frac{(\bar{\rho}_h)_i^{n+1,1}}{(\bar{\rho}_h)_i^{n+1,1} - m_i}, \frac{1 - (\bar{\rho}_h)_i^{n+1,1}}{M_i - (\bar{\rho}_h)_i^{n+1,1}}, 1 \right\},$$

$$m_i = \min \rho_h^{n+1,1}(x_{i\pm\frac{1}{2}}^\mp), \quad M_i = \max \rho_h^{n+1,1}(x_{i\pm\frac{1}{2}}^\mp).$$

Then we get  $\rho_h^{n+1,2}(x_{i\pm\frac{1}{2}}^\mp) \in [0, 1]$  and  $(\bar{\rho}_h)_i^{n+1,2} = (\bar{\rho}_h)_i^{n+1,1}$  (see [32]). Furthermore,  
the interpolation polynomial of  $\{\rho_h^{n+1,2}(x_{i\pm\frac{1}{2}}^\mp)\}$  on  $I_i$  satisfies

$$\left| \rho_h^{n+1,2}(x) - \rho_h^{n+1,1}(x) \right| \leq C_k \max_{x \in \{x_{i\pm\frac{1}{2}}^\mp\}} \left| \rho(x, t_{n+1}) - \rho_h^{n+1,1}(x) \right|,$$

265 where  $\rho(x, t_{n+1})$  is the exact solution at time  $t_{n+1}$  and  $C_k$  is a constant depending  
266 only on the polynomial degree  $k$ . Consequently, we can update

$$267 \quad \rho_h^{n+1} = e^{\tau \mathcal{L}(\rho_h^n)} \rho_h^{n+1,2}.$$

268 and conclude that  $\rho_h^{n+1} \in [0, 1]$  by Lemma 2.2. Denote the bound limiter as  $\mathcal{P}$ . The  
269 first-order bound-preserving scheme can be summarized as

$$270 \quad (3.14) \quad \rho_h^{n+1} = e^{\tau \mathcal{L}(\rho_h^n)} \mathcal{P}(\rho_h^n + \tau \mathcal{N}_h(\rho_h^n)).$$

271 Using the approximation (3.13), a more efficient first-order scheme is given by

$$272 \quad (3.15) \quad \rho_h^{n+1} = (I - \tau \mathcal{L}(\rho_h^n))^{-1} \mathcal{P}(\rho_h^n + \tau \mathcal{N}_h(\rho_h^n)).$$

273

274 **THEOREM 3.4.** *The updates (3.14) and (3.15) are bound preserving and mass*  
275 *conservative, provided the time step restriction specified in Lemma 3.1 is satisfied.*

276 **3.2. Second-order scheme.** Based on the first-order scheme (3.14) or (3.15),  
277 we can construct a first-order approximation for  $\mathcal{L}_h(\rho_h)$ . Specially, let

$$278 \quad (3.16a) \quad \rho_h^{n+1,1} = \rho_h^n + \tau \mathcal{N}_h(\rho_h^n),$$

$$279 \quad (3.16b) \quad \tilde{\rho}_h^{n+1} = (I - \tau \mathcal{L}_h(\rho_h^n))^{-1} \rho_h^{n+1,1},$$

281 and introduce the linear interpolation

$$282 \quad (3.17) \quad L_1(t) = \frac{t - t_n}{\tau} \mathcal{L}_h(\tilde{\rho}_h^{n+1}) + \left( 1 - \frac{t - t_n}{\tau} \right) \mathcal{L}_h(\rho_h^n),$$

283 which provides a first approximation for  $\mathcal{L}_h(\boldsymbol{\rho}_h)$  on the interval  $[t_n, t_{n+1}]$ . Conse-  
284 quently, the integrating factor (3.3) becomes

$$285 \quad (3.18) \quad \mathcal{T}(t) = \frac{(t-t_n)^2}{2\tau} \mathcal{L}_h(\tilde{\boldsymbol{\rho}}_h^{n+1}) - \frac{\tau}{2} \left(1 - \frac{t-t_n}{\tau}\right)^2 \mathcal{L}_h(\boldsymbol{\rho}_h^n).$$

286 Applying the second-order SSP Runge-Kutta [18] for (3.4), we obtain the scheme

$$287 \quad (3.19a) \quad \boldsymbol{\rho}_h^{n+1,2} = e^{\tau \tilde{\mathcal{L}}_h^{n+1}} \boldsymbol{\rho}_h^{n+1,1},$$

$$288 \quad (3.19b) \quad \boldsymbol{\rho}_h^{n+1} = \frac{1}{2} e^{\tau \tilde{\mathcal{L}}_h^{n+1}} \boldsymbol{\rho}_h^n + \frac{1}{2} \left( \boldsymbol{\rho}_h^{n+1,2} + \tau \mathcal{N}_h(\boldsymbol{\rho}_h^{n+1,2}) \right),$$

290 where

$$291 \quad \tilde{\mathcal{L}}_h^{n+1} = \frac{1}{2} (\mathcal{L}(\tilde{\boldsymbol{\rho}}_h^{n+1}) + \mathcal{L}_h(\boldsymbol{\rho}_h^n)).$$

292 *Remark 3.5.* Due to the properties  $L_1(t_n) = \mathcal{L}_h(\boldsymbol{\rho}_h^n)$  and  $L_1(t_{n+1}) = \mathcal{L}_h(\tilde{\boldsymbol{\rho}}_h^{n+1})$ ,  
293 the stiff term  $\mathcal{L}_h(\boldsymbol{\rho}_h)\boldsymbol{\rho}_h$  does not appear in the explicit Euler steps (3.16a) and (3.19b),  
294 even though it exists in the ODE (3.5). Hence, the stability of the explicit Euler step  
295 only depends on the nonlinear term  $\mathcal{N}_h$ .

296 Let  $\boldsymbol{\rho}_h(t)$  be an exact solution for (2.5), we next show that (3.19) is second-order  
297 in time. Denote  $\mathcal{G}(\boldsymbol{\rho}_h) = \mathcal{L}_h(\boldsymbol{\rho}_h)\boldsymbol{\rho}_h + \mathcal{N}_h(\boldsymbol{\rho}_h)$  and  $\boldsymbol{\rho} = \boldsymbol{\rho}_h(t_n)$  for simplicity. The  
298 Taylor's expansion gives that

(3.20)

$$\begin{aligned} \boldsymbol{\rho}_h(t_{n+1}) &= \boldsymbol{\rho} + \tau \mathcal{G}(\boldsymbol{\rho}) + \frac{\tau^2}{2} \mathcal{G}_t(\boldsymbol{\rho}) + O(\tau^3) \\ &= \boldsymbol{\rho} + \tau \mathcal{G}(\boldsymbol{\rho}) + \frac{\tau^2}{2} ((\mathcal{L}'_h(\boldsymbol{\rho})\mathcal{G}(\boldsymbol{\rho}))\boldsymbol{\rho} + \mathcal{L}_h(\boldsymbol{\rho})\mathcal{G}(\boldsymbol{\rho})) + \tau^2 \mathcal{N}'_h(\boldsymbol{\rho})\mathcal{G}(\boldsymbol{\rho}) + O(\tau^3) \end{aligned}$$

300 Substitute the exact solution into (3.16) and (3.19), we get

$$301 \quad \tilde{\boldsymbol{\rho}}_h^{n+1} = \boldsymbol{\rho} + \tau \mathcal{G}(\boldsymbol{\rho}) + O(\tau^2)$$

$$302 \quad \mathcal{L}_h(\tilde{\boldsymbol{\rho}}_h^{n+1}) = \mathcal{L}_h(\boldsymbol{\rho}) + \tau \mathcal{L}'_h(\boldsymbol{\rho})\mathcal{G}(\boldsymbol{\rho}) + O(\tau^2)$$

$$303 \quad \boldsymbol{\rho}_h^{n+1,2} = \boldsymbol{\rho} + \tau \left( \tilde{\mathcal{L}}_h^{n+1} \boldsymbol{\rho} + \mathcal{N}_h(\boldsymbol{\rho}) \right) + \frac{\tau^2}{2} \tilde{\mathcal{L}}_h^{n+1} \left( \tilde{\mathcal{L}}_h^{n+1} \boldsymbol{\rho} + 2\mathcal{N}_h(\boldsymbol{\rho}) \right) + O(\tau^3)$$

$$304 \quad = \boldsymbol{\rho} + \tau \mathcal{G}(\boldsymbol{\rho}) + \frac{\tau^2}{2} \mathcal{L}_h(\boldsymbol{\rho}) (\mathcal{G}(\boldsymbol{\rho}) + \mathcal{N}_h(\boldsymbol{\rho})) + \frac{\tau}{2} (\mathcal{L}_h(\tilde{\boldsymbol{\rho}}_h^{n+1}) - \mathcal{L}_h(\boldsymbol{\rho}))\boldsymbol{\rho} + O(\tau^3)$$

$$305 \quad = \boldsymbol{\rho} + \tau \mathcal{G}(\boldsymbol{\rho}) + \frac{\tau^2}{2} \mathcal{L}_h(\boldsymbol{\rho}) (\mathcal{G}(\boldsymbol{\rho}) + \mathcal{N}_h(\boldsymbol{\rho})) + \frac{\tau^2}{2} (\mathcal{L}'_h(\boldsymbol{\rho})\mathcal{G}(\boldsymbol{\rho}))\boldsymbol{\rho} + O(\tau^3)$$

$$306 \quad \mathcal{N}_h(\boldsymbol{\rho}_h^{n+1,2}) = \mathcal{N}_h(\boldsymbol{\rho}) + \tau \mathcal{N}'_h(\boldsymbol{\rho})\mathcal{G}(\boldsymbol{\rho}) + O(\tau^2)$$

$$307 \quad \boldsymbol{\rho}_h^{n+1} = \frac{1}{2} \left( I + \tau \tilde{\mathcal{L}}_h^{n+1} + \frac{\tau^2}{2} (\tilde{\mathcal{L}}_h^{n+1})^2 \right) \boldsymbol{\rho} + \frac{1}{2} \left( \boldsymbol{\rho}_h^{n+1,2} + \tau \mathcal{N}_h(\boldsymbol{\rho}_h^{n+1,2}) \right) + O(\tau^3)$$

$$308 \quad = \boldsymbol{\rho} + \frac{\tau}{2} (\mathcal{L}_h(\boldsymbol{\rho})\boldsymbol{\rho} + \mathcal{N}_h(\boldsymbol{\rho})) + \frac{\tau^2}{4} (\mathcal{L}_h(\boldsymbol{\rho}))^2 \boldsymbol{\rho} + \frac{1}{2} (\boldsymbol{\rho}_h^{n+1,2} - \boldsymbol{\rho})$$

$$309 \quad + \frac{\tau}{4} (\mathcal{L}_h(\tilde{\boldsymbol{\rho}}_h^{n+1}) - \mathcal{L}_h(\boldsymbol{\rho}))\boldsymbol{\rho} + \frac{\tau}{2} (\mathcal{N}_h(\boldsymbol{\rho}_h^{n+1,2}) - \mathcal{N}_h(\boldsymbol{\rho})) + O(\tau^3)$$

$$310 \quad = \boldsymbol{\rho} + \tau \mathcal{G}(\boldsymbol{\rho}) + \frac{\tau^2}{4} (\mathcal{L}_h(\boldsymbol{\rho}))^2 \boldsymbol{\rho} + \frac{\tau^2}{4} \mathcal{L}_h(\boldsymbol{\rho}) (\mathcal{G}(\boldsymbol{\rho}) + \mathcal{N}_h(\boldsymbol{\rho}))$$

$$\begin{aligned}
& + \frac{\tau^2}{2} (\mathcal{L}'_h(\boldsymbol{\rho})\mathcal{G}(\boldsymbol{\rho})) \boldsymbol{\rho} + \frac{\tau^2}{2} \mathcal{N}'_h(\boldsymbol{\rho})\mathcal{G}(\boldsymbol{\rho}) + O(\tau^3) \\
& = \boldsymbol{\rho} + \tau\mathcal{G}(\boldsymbol{\rho}) + \frac{\tau^2}{2} ((\mathcal{L}'_h(\boldsymbol{\rho})\mathcal{G}(\boldsymbol{\rho})) \boldsymbol{\rho} + \mathcal{L}_h(\boldsymbol{\rho})\mathcal{G}(\boldsymbol{\rho})) + \frac{\tau^2}{2} \mathcal{N}'_h(\boldsymbol{\rho})\mathcal{G}(\boldsymbol{\rho}) + O(\tau^3).
\end{aligned}$$

Together with (3.20), one has

$$\boldsymbol{\rho}_h(t_{n+1}) - \boldsymbol{\rho}_h^{n+1} = O(\tau^3),$$

which implies that the scheme (3.19) is a second-order temporal discretization for ODE (2.5). When the bound-preserving limiter is applied immediately after each Euler forward stage, we obtain a second-order bound-preserving scheme

$$(3.21a) \quad \boldsymbol{\rho}_h^{n+1,1} = (I - \tau\mathcal{L}_h(\boldsymbol{\rho}_h^n))^{-1} \mathcal{P}(\boldsymbol{\rho}_h^n + \tau\mathcal{N}_h(\boldsymbol{\rho}_h^n)),$$

$$(3.21b) \quad \boldsymbol{\rho}_h^{n+1,2} = e^{\frac{\tau}{2}(\mathcal{L}_h(\boldsymbol{\rho}_h^n) + \mathcal{L}_h(\boldsymbol{\rho}_h^{n+1,1}))} \mathcal{P}(\boldsymbol{\rho}_h^n + \tau\mathcal{N}_h(\boldsymbol{\rho}_h^n)),$$

$$(3.21c) \quad \boldsymbol{\rho}_h^{n+1} = \frac{1}{2} e^{\frac{\tau}{2}(\mathcal{L}_h(\boldsymbol{\rho}_h^n) + \mathcal{L}_h(\boldsymbol{\rho}_h^{n+1,1}))} \boldsymbol{\rho}_h^n + \frac{1}{2} \mathcal{P}(\boldsymbol{\rho}_h^{n+1,2} + \tau\mathcal{N}_h(\boldsymbol{\rho}_h^{n+1,2})).$$

Similar to the first-order scheme (3.14), we have the following theorem for (3.21).

**THEOREM 3.6.** *The time discretization (3.21) of the semi-discrete scheme (2.5) is bound preserving and mass conservative as long as the time step restriction in Lemma 3.1 is satisfied.*

**Remark 3.7.** For practical implementation, one can use the second-order approximation

$$(3.22) \quad e^{\tau\mathcal{L}} \approx \left( I - \tau\mathcal{L} + \frac{\tau^2}{2}\mathcal{L}^2 \right)^{-1}$$

in (3.21) to optimize computational efficiency. However, the guarantee of bound-preservation is compromised due to the inclusion of  $\mathcal{L}^2$ . A pragmatic approach would be to initially utilize the approximation from (3.22). If a value surpasses the expected density bounds, the respective step should be discarded. Subsequently, one should revert to computing using the exponential matrix.

**4. Numerical results.** In this section, we examine the performance and accuracy of our proposed numerical schemes (3.21) for computing several examples on domain  $\Omega = [-L, L]^d$ ,  $d = 1, 2$ . The error is measured in the discrete norms

$$\begin{aligned}
(4.1) \quad err_{L^1} &= \widetilde{\int}_{\Omega} |\rho_h(\mathbf{x}, t) - \rho(\mathbf{x}, t)| d\mathbf{x} = \left(\frac{h}{2}\right)^d \|\boldsymbol{\rho}_h - \boldsymbol{\rho}\|_{\ell^1}, \\
err_{L^2} &= \sqrt{\widetilde{\int}_{\Omega} |\rho_h(\mathbf{x}, t) - \rho(\mathbf{x}, t)|^2 d\mathbf{x}} = \left(\frac{h}{2}\right)^{\frac{d}{2}} \|\boldsymbol{\rho}_h - \boldsymbol{\rho}\|_{\ell^2}, \\
err_{L^\infty} &= \|\boldsymbol{\rho}_h - \boldsymbol{\rho}\|_{\infty}.
\end{aligned}$$

Here  $\rho_h$  is the numerical solution obtained by the scheme (3.21), and  $\rho$  is the exact solution for (1.1) or a reference solution computed by our approach in a finer mesh. Vectors  $\boldsymbol{\rho}_h$  and  $\boldsymbol{\rho}$  are the values of  $\rho_h$  and  $\rho$  on all Gauss-Lobatto quadrature points, respectively. We chose  $g = \rho$  in the flux (2.3) and use CFL condition  $\tau = \frac{1}{4L}h$  for all following numerical tests. The exponential matrix is efficiently calculated by the techniques introduced in [20].

345 **4.1. Accuracy test.** We first examine the accuracy of (3.21) on an initial value  
 346 problem with a source term  $S$ :

$$347 \quad (4.2) \quad \begin{cases} \rho_t = \nabla \rho (1 - \rho) \nabla (\rho + \sin(\mathbf{1}^\top \mathbf{x}) + W * \rho) + S(\mathbf{x}, t), & \mathbf{x} \in [-\pi, \pi]^d, t > 0, \\ \rho(\mathbf{x}, 0) = \frac{1}{4} (\sin(\mathbf{1}^\top \mathbf{x}) + 1), \end{cases}$$

348 where  $\mathbf{1} = (1, \dots, 1)^\top \in \mathbb{R}^d$  and  $W(\mathbf{x}) = \cos(\mathbf{1}^\top \mathbf{x}) / (2\pi)$ . Here periodic boundary  
 349 conditions are applied and the source term  $S$  is used to ensure that the exact solution  
 350 is

$$351 \quad (4.3) \quad \rho(\mathbf{x}, t) = \frac{1}{4} (\sin(\mathbf{1}^\top \mathbf{x} + t) + 1).$$

352 In this test,  $F = f = \rho(1 - \rho)$ ,  $H' = \rho$  and  $V = \sin(\mathbf{1}^\top \mathbf{x})$ . We calculate the error at  
 353  $T = 1$ . Table 1 and Table 2 show the corresponding second-order convergence in one  
 354 and two dimensions.

TABLE 1

*Accuracy test in one dimension for computing a solution to the equation (4.2). The error is calculated at  $T = 1$ .*

$N$	$L^1$ error	Order	$L^2$ error	Order	$L^\infty$ error	Order
20	2.074e-02		9.966e-03		8.508e-03	
40	5.032e-03	2.043	2.442e-03	2.029	2.639e-03	1.689
80	1.232e-03	2.030	6.006e-04	2.024	6.788e-04	1.959
160	3.029e-04	2.024	1.463e-04	2.038	1.752e-04	1.954

TABLE 2

*Accuracy test in two dimensions for computing a solution to the equation (4.2). The error is calculated at  $T = 1$ .*

$N$	$L^1$ error	Order	$L^2$ error	Order	$L^\infty$ error	Order
$10 \times 10$	9.177e-01		1.884e-01		1.051e-01	
$20 \times 20$	2.182e-01	2.073	4.636e-02	2.023	3.046e-02	1.787
$40 \times 40$	5.095e-02	2.098	1.038e-02	2.159	6.019e-03	2.339

355 **4.2. Saturation experiment.** To demonstrate the bound-preserving property  
 356 of our numerical scheme, we consider the saturation experiment given by

$$357 \quad (4.4) \quad \begin{cases} \rho_t = \nabla \left( \rho(1 - \rho) \nabla \left( D \ln(\rho) + \frac{C}{2} |\mathbf{x}|^2 \right) \right), \\ \rho(\mathbf{x}, 0) = \rho_0. \end{cases}$$

358 Here  $D$  and  $C$  are positive numbers. In this case,  $f = \rho(1 - \rho)$ ,  $H = D(\rho \ln(\rho) - \rho)$ ,  
 359  $F = fH'' = D(1 - \rho)$ ,  $V(x) = \frac{C}{2} |\mathbf{x}|^2$  and  $W(\mathbf{x}) = 0$ . The exact solution of (4.4) is  
 360 bounded on  $[0, 1]$  and the steady state depends on the initial mass  $m = \|\rho_0\|_{L^1}$ . There  
 361 exists a threshold  $m_c = (\frac{2\pi D}{C})^{d/2}$  such that the steady state can be written as

$$362 \quad (4.5) \quad \rho_\infty(\mathbf{x}) = \begin{cases} A \exp\left(-\frac{C}{2D} |\mathbf{x}|^2\right), & m \leq m_c \\ B \exp\left(-\frac{C}{2D} \max\{|\mathbf{x}|^2 - \ell^2, 0\}\right), & m > m_c \end{cases}$$

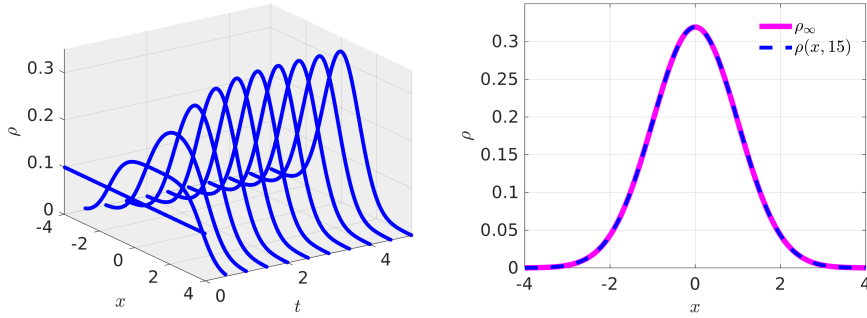


FIG. 1. Computation of a smooth solution to the one-dimensional saturation experiment (4.4) with  $\rho_0 \equiv 0.1$ . **Left:** Evolution of  $\rho_h(x,t)$ ; **Right:** Comparison between  $\rho_\infty$  and the numerical solution calculated at  $T = 15$ ;

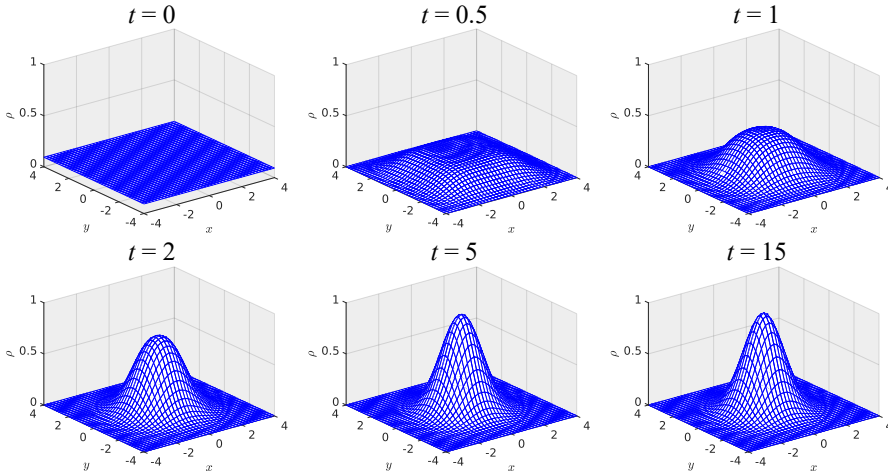


FIG. 2. Evolution of a solution  $\rho(\mathbf{x},t)$  with  $\rho_0 \equiv 0.09375$  in a two-dimensional saturation experiment (4.4).

363 where  $A, B$  are positive constants such that  $\|\rho_\infty\|_{L^1} = \|\rho_0\|_{L^1} = m$ , and  $\ell$  can be  
 364 determined from the initial datum (see reference [1]). Numerically, we solve the equa-  
 365 tion (4.4) over the domain  $\Omega = [-4, 4]^d$  with parameters  $C = 1, D = 1$ . Consequently,  
 366 the threshold  $m_c = (2\pi)^{d/2}$  in (4.5).

367 To verify the convergence order, we begin with a uniform initial data  $\rho_0 \equiv 0.1$  in  
 368 one dimension and  $\rho_0 \equiv 0.09375$  in two dimensions. This ensures that  $\|\rho_0\|_{L^1} \leq m_c$   
 369 and leads to a smooth steady state according to (4.5). We then calculate the numerical  
 370 solution at  $T = 15$  as the numerical steady state. Figure 1 and Figure 2 illustrate  
 371 the numerical evolution to the steady state in one and two dimensions, respectively.  
 372 Furthermore, Table 5 and Table 4 demonstrate the anticipated second-order accuracy  
 373 in both one and two dimensions. In Figure 3, we present the behavior of the relative  
 374 entropy  $E(t|\infty) = E(\rho_h(t)) - E(\rho_\infty)$  and the associated bound of our solution. The  
 375 results indicate that our scheme preserves the bound, aligning with our theoretical  
 376 analysis, and also exhibits energy dissipation during this test.

377 To observe saturation, we begin with a uniform initial density of  $\rho_0 \equiv 0.415$  in

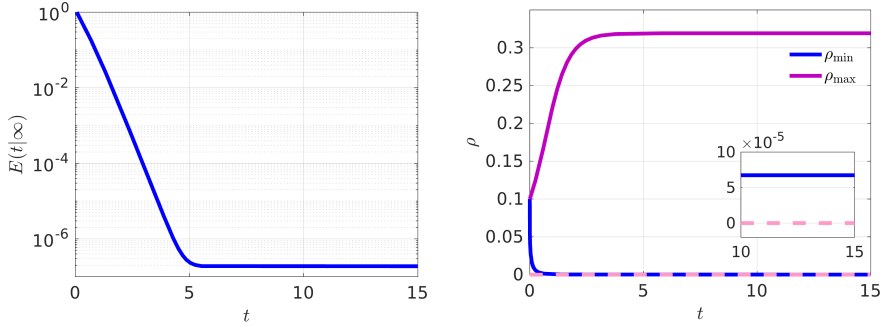


FIG. 3. Computation of a smooth solution to the one-dimensional saturation experiment (4.4) with  $\rho_0 = 0.1$ . **Left:** Behaviour of the relative energy  $E(t; \infty)$ ; **Right:** Behaviour of bound.

TABLE 3

Accuracy test in one dimension for computing the steady state to the equation (4.4) with a uniform initial density  $\rho_0 \equiv 0.1$ . The error is calculated at  $T = 15$ .

$N$	$L^1$ error	Order	$L^2$ error	Order	$L^\infty$ error	Order
20	2.091e-02		9.166e-03		6.682e-03	
40	2.055e-03	3.347	9.324e-04	3.297	7.039e-04	3.247
80	5.159e-04	1.994	2.234e-04	2.062	1.557e-04	2.176
160	1.299e-04	1.989	5.502e-05	2.021	3.624e-05	2.103

TABLE 4

Accuracy test in two dimensions for computing a smooth steady state to the equation (4.4) with uniform initial density  $\rho_0 \equiv 0.09375$ . The error is calculated at  $T = 15$

$N$	$L^1$ error	Order	$L^2$ error	Order	$L^\infty$ error	Order
$10 \times 10$	5.152e-01		8.907e-02		2.554e-02	
$20 \times 20$	1.436e-01	1.843	2.486e-02	1.841	9.420e-03	1.439
$40 \times 40$	3.032e-02	2.243	5.063e-03	2.296	2.062e-03	2.192

378 one dimension and  $\rho_0 \equiv 0.147$  in two dimensions such that  $\|\rho_0\|_{L^1} > m_c$ . According  
379 to (4.5), this initial density results in a non-smooth steady state that is bounded  
380 between 0 and 1. A numerical solution obtained at  $T = 15$  is considered as the  
381 numerical steady state. The evolution in both one and two dimensions can be found  
382 in Figure 4 and Figure 5. As depicted in Figure 4, in contrast to the results from [9,  
383 Section 4.1], our DG discretization method yields a superior approximation devoid of  
384 oscillations near the upper bound  $\rho_{\max} = 1$ . Additionally, we present the behavior  
385 of the relative entropy and the bound in Figure 6, which shows that the numerical  
386 solution generated by our scheme demonstrates bound preservation within the interval  
387  $[0, 1]$  and also exhibits entropy dissipation. In order to test the accuracy of this  
388 example, we calculated the error at  $T = 1$ , employing reference solutions calculated  
389 at a finer mesh size with  $N = 320$  for one-dimensional computations and  $N = 80 \times 80$   
390 for two-dimensional computations. Table 5 and Table 6 present the second-order  
391 accuracy of our approach in both one and two dimensions.

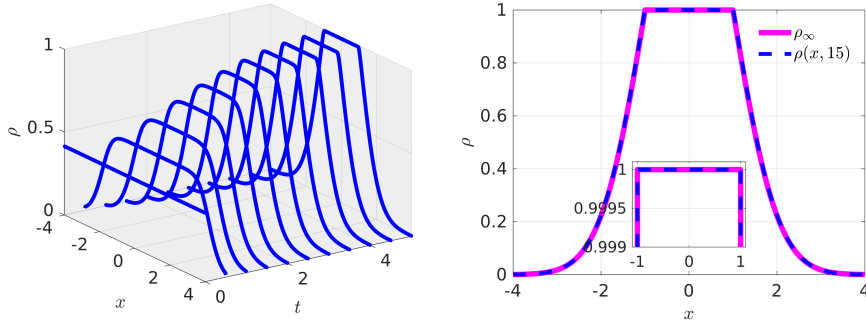


FIG. 4. Computation of a non-smooth steady state to the one-dimensional saturation experiment (4.4) with  $\rho_0 = 0.415$ . **Left:** Evolution of  $\rho(x, t)$ ; **Right:** Comparison between  $\rho_\infty$  and the numerical solution calculated at  $T = 15$ .

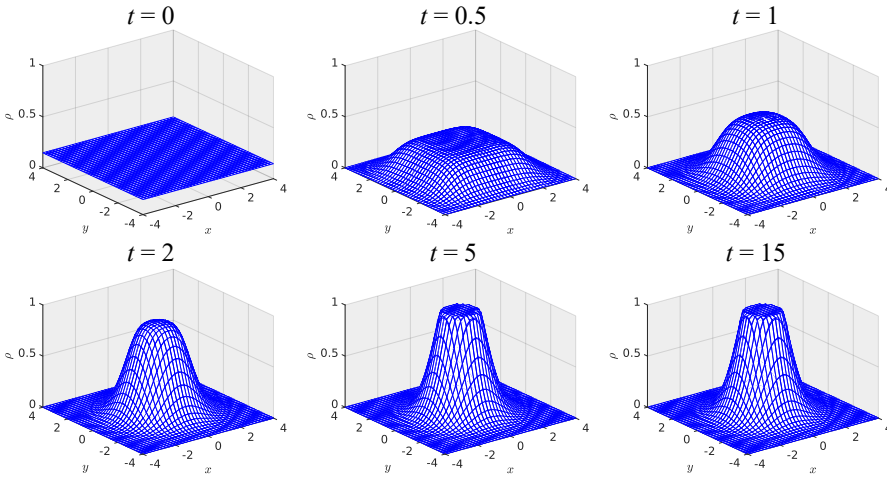


FIG. 5. Evolution of a solution  $\rho(\mathbf{x}, t)$  with  $\rho_0 = 0.147$  in a two-dimensional saturation experiment (4.4).

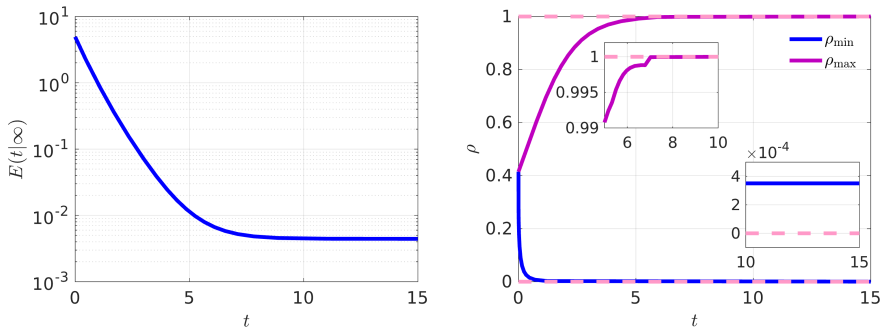


FIG. 6. Computation of a non-smooth steady state to the one-dimensional saturation experiment (4.4) with  $\rho_0 = 0.415$ . **Left:** Behaviour of the relative entropy  $E(t, \infty)$ ; **Right:** Behaviour of bound.

TABLE 5

Accuracy test in one dimension for computing a solution to the equation (4.4) with uniform initial density  $\rho_0 \equiv 0.415$ . The error is calculated at  $T = 1$ .

$N$	$L^1$ error	Order	$L^2$ error	Order	$L^\infty$ error	Order
20	3.022e-02		1.467e-02		1.158e-02	
40	7.603e-03	1.991	3.811e-03	1.944	4.007e-03	1.531
80	1.789e-03	2.088	8.774e-04	2.119	9.146e-04	2.131
160	3.669e-04	2.285	1.792e-04	2.291	1.775e-04	2.365

TABLE 6

Accuracy test in two dimensions for computing a solution to the equation (4.4) with uniform initial density  $\rho_0 = 0.147$ . The error is calculated at  $T = 1$ .

$N$	$L^1$ error	Order	$L^2$ error	Order	$L^\infty$ error	Order
$10 \times 10$	5.152e-01		8.897e-02		2.555e-02	
$20 \times 20$	1.436e-01	1.843	2.483e-02	1.841	9.405e-03	1.442
$40 \times 40$	3.032e-02	2.244	5.057e-03	2.296	2.059e-03	2.191

392 **4.3. Aggregation–diffusion equation.** We proceed with our study of the  
 393 scheme (3.21) on the aggregation-diffusion equation

$$394 \quad (4.6) \quad \rho_t = \nabla \rho \nabla \left( \frac{\nu m}{m-1} \rho^{m-1} + W * \rho \right) = \nu \Delta \rho^m + \nabla \rho \nabla (W * \rho)$$

395 with interaction kernel  $W = e^{|\mathbf{x}|^2} / (2\pi)^{d/2}$ . The parameters  $\nu > 0$  and  $m > 1$  are set  
 396 to  $\nu = 0.05$  and  $m = 3$  in our computation. In this example,  $f = \rho$ ,  $F = \nu m \rho^{m-1}$ ,  
 397  $V = 0$ , and the density  $\rho$  remains positive. For our tests, we utilize periodic boundary  
 398 conditions and evaluate the solution over the domain  $[-6, 6]$  in one dimension and  
 399  $[-4, 4]^2$  in two dimensions.

400 For the one-dimensional test, we compute the solution up to time  $T = 200$ , using a  
 401 smooth initial datum  $\rho_0 = \frac{1}{\sqrt{2\pi}}(e^{-(x-2)^2/2} + e^{-(x+2)^2/2})$ . The evolution and behavior  
 402 of entropy are plotted in Figure 7. As time progresses, the density starts at a smooth  
 403 initial state with two peaks and then converges to a non-smooth steady state with only  
 404 one peak and two discontinuity points. The entropy also shows dissipation throughout  
 405 the computation. To ascertain the accuracy of this example, we compute the error at  
 406  $T = 1$  and refer to a benchmark solution computed with a mesh of  $N = 320$  points.  
 407 Table 7 demonstrates the desired second-order accuracy of our scheme (3.21).

TABLE 7

Accuracy test in one dimension for computing a solution to the equation (4.6) with  $\rho_0 = \frac{1}{\sqrt{2\pi}}(e^{-(x-2)^2/2} + e^{-(x+2)^2/2})$ . The error is calculated at  $T = 1$ .

$N$	$L^1$ error	Order	$L^2$ error	Order	$L^\infty$ error	Order
20	3.993e-02		1.489e-02		9.097e-03	
40	1.608e-02	1.312	5.739e-03	1.376	3.056e-03	1.574
80	4.900e-03	1.714	1.742e-03	1.720	9.306e-04	1.715
160	1.040e-03	2.236	3.772e-04	2.208	2.113e-04	2.139

408 In two dimensions, we consider a test with a discontinuous initial state given by  
 409  $\rho_0(\mathbf{x}) = 1_{[-2,2] \times [-2,2]}(\mathbf{x})$ . Figure 8 shows the dynamic evolution used to compute a



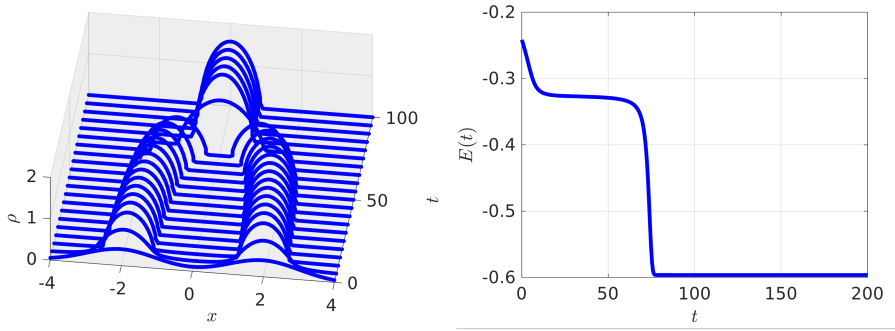


FIG. 7. Computation of a steady state to the one-dimensional aggregation-diffusion equation (4.6) with  $\rho_0 = \frac{1}{\sqrt{2\pi}}(e^{-(x-2)^2/2} + e^{-(x+2)^2/2})$ . **Left:** Evolution of  $\rho(x,t)$ ; **Right:** Behaviour of the discrete entropy.

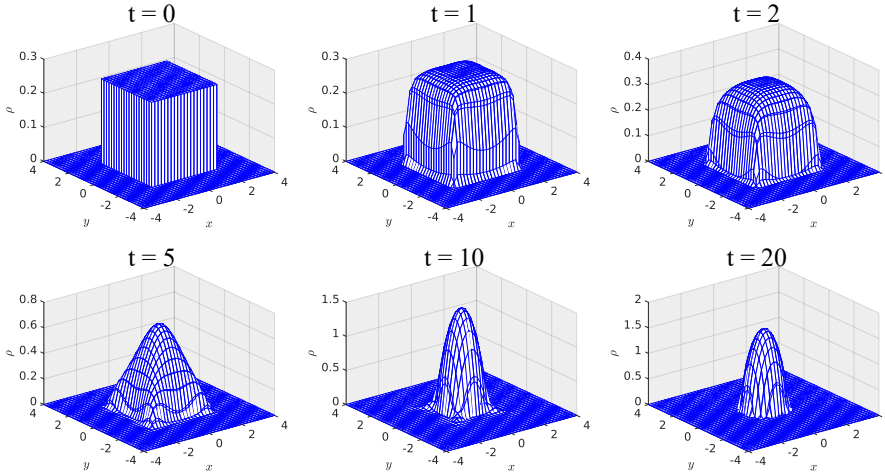


FIG. 8. Evolution of a solution  $\rho(\mathbf{x},t)$  to a two-dimensional aggregation-diffusion equation (4.6) with  $\rho_0 = 1_{[-2,2] \times [-2,2]}$ .

410 solution at  $T = 20$  with  $N = 40 \times 40$  cells. In this setting,  $\rho$  exhibits a transition from  
 411 a discontinuous distribution to a concentrated central peak. To test the accuracy in  
 412 this two-dimensional case, we computed the error at  $T = 1$  with a reference solution  
 413 calculated using a mesh of  $N = 80 \times 80$  cells. The error table and convergence rate  
 414 are provided in Table 8. In this example, the  $L^1$  error shows second-order accuracy,  
 415 while the observed degeneracy in  $L^2$  and  $L^\infty$  accuracy is due to the discontinuity in  
 416 the initial state and the non-smoothness of the solution.

417 **Conclusions.** This paper presented a fully discrete scheme for solving a class  
 418 of degenerate parabolic equations. Spatially, we applied a discontinuous Galerkin  
 419 method to an appropriate reformulation of equations, resulting in an ODE with a  
 420 splitting structure. Our numerical examples demonstrated that this spatial discretiza-  
 421 tion induces fewer oscillations in the solution. Temporally, we proposed a second-order  
 422 exponential scheme, which involves only linear solvers, by introducing integrating fac-  
 423 tors into the ODE and utilizing SSP-RK methods. Notably, our approach consistently

TABLE 8

Accuracy test in two dimensions for computing a solution to the equation (4.6) with  $\rho_0 = 1_{[-2,2] \times [-2,2]}$ . The error is calculated at  $T = 1$ .

$N$	$L^1$ error	Order	$L^2$ error	Order	$L^\infty$ error	Order
$10 \times 10$	1.674e+00		5.822e-01		2.587e-01	
$20 \times 20$	4.250e-01	1.978	1.899e-01	1.616	1.188e-01	1.124
$40 \times 40$	1.110e-01	1.937	6.151e-02	1.627	5.446e-02	1.125

evidences second-order accuracy, bound preservation and mass conservation with a favorable CFL condition  $\tau \sim h$  both in theory and in practice. Nevertheless, the calculation of the exponential matrix partly limited our efficiency, and energy dissipation was only shown in our numerical tests but not proved theoretically. Indeed, devising an efficient linear scheme that simultaneously provides high-order accuracy in both space and time, while guaranteeing bound preservation, mass conservation, and energy dissipation, continues to be a major challenge.

**Acknowledgments.** The first author would like to acknowledge the Tsinghua Scholarship for Overseas Graduate Students (No. 2022118) for financial support and advisors Profs. Chi-Wang Shu and Chenglong Bao for their invaluable guidance.

434

## REFERENCES

- [1] R. BAILO, J. A. CARRILLO, AND J. HU, *Bound-preserving finite-volume schemes for systems of continuity equations with saturation*, SIAM Journal on Applied Mathematics, 83 (2023), pp. 1315–1339.
- [2] R. BAILO, J. A. CARRILLO, H. MURAKAWA, AND M. SCHMIDTCHEN, *Convergence of a fully discrete and energy-dissipating finite-volume scheme for aggregation-diffusion equations*, Mathematical Models and Methods in Applied Sciences, 30 (2020), pp. 2487–2522.
- [3] M. BESSEMOULIN-CHATARD AND F. FILBET, *A finite volume scheme for nonlinear degenerate parabolic equations*, SIAM Journal on Scientific Computing, 34 (2012), pp. B559–B583.
- [4] S. BLANES, A. ISERLES, AND S. MACNAMARA, *Positivity-preserving methods for ordinary differential equations*, ESAIM: Mathematical Modelling and Numerical Analysis, 56 (2022), pp. 1843–1870.
- [5] S. BOSCARINO, R. BÜRGER, P. MULET, G. RUSSO, AND L. M. VILLADA, *Linearly implicit IMEX Runge–Kutta methods for a class of degenerate convection-diffusion problems*, SIAM Journal on Scientific Computing, 37 (2015), pp. B305–B331.
- [6] R. BÜRGER, D. INZUNZA, P. MULET, AND L. M. VILLADA, *Implicit-explicit methods for a class of nonlinear nonlocal gradient flow equations modelling collective behaviour*, Applied Numerical Mathematics, 144 (2019), pp. 234–252.
- [7] M. CALIARI, F. CASSINI, L. EINKEMMER, AND A. OSTERMANN, *Accelerating exponential integrators to efficiently solve advection-diffusion-reaction equations*, arXiv preprint arXiv:2303.15861, (2023).
- [8] J. A. CARRILLO, K. CRAIG, AND Y. YAO, *Aggregation-diffusion equations: dynamics, asymptotics, and singular limits*, Active Particles, Volume 2: Advances in Theory, Models, and Applications, (2019), pp. 65–108.
- [9] J. A. CARRILLO, L. WANG, AND C. WEI, *Structure preserving primal dual methods for gradient flows with nonlinear mobility transport distances*, SIAM Journal on Numerical Analysis, accepted (2023).
- [10] Q. CHENG AND J. SHEN, *A new Lagrange multiplier approach for constructing structure preserving schemes, II. Bound preserving*, SIAM Journal on Numerical Analysis, 60 (2022), pp. 970–998.
- [11] A. CHERTOCK, S. CUI, A. KURGANOV, AND T. WU, *Steady state and sign preserving semi-implicit Runge–Kutta methods for ODEs with stiff damping term*, SIAM Journal on Numerical Analysis, 53 (2015), pp. 2008–2029.
- [12] C. CLANCY AND J. A. PUDYKIEWICZ, *On the use of exponential time integration methods in atmospheric models*, Tellus A: Dynamic Meteorology and Oceanography, 65 (2013),

- 469 p. 20898.
- 470 [13] Q. DU, L. JU, X. LI, AND Z. QIAO, *Maximum bound principles for a class of semilinear*  
471 *parabolic equations and exponential time-differencing schemes*, SIAM Review, 63 (2021),  
472 pp. 317–359.
- 473 [14] C. DUAN, W. CHEN, C. LIU, X. YUE, AND S. ZHOU, *Structure-preserving numerical methods for*  
474 *nonlinear Fokker–Planck equations with nonlocal interactions by an energetic variational*  
475 *approach*, SIAM Journal on Scientific Computing, 43 (2021), pp. B82–B107.
- 476 [15] L. EINKEMMER, M. TOKMAN, AND J. LOFFELD, *On the performance of exponential integrators*  
477 *for problems in magnetohydrodynamics*, Journal of Computational Physics, 330 (2017),  
478 pp. 550–565.
- 479 [16] C. M. ELLIOTT AND H. GARCKE, *On the Cahn–Hilliard equation with degenerate mobility*,  
480 SIAM Journal on Mathematical Analysis, 27 (1996), pp. 404–423.
- 481 [17] S. GOTTLIEB, Z. J. GRANT, J. HU, AND R. SHU, *High order strong stability preserving multi-*  
482 *derivative implicit and IMEX Runge–Kutta methods with asymptotic preserving properties*,  
483 SIAM Journal on Numerical Analysis, 60 (2022), pp. 423–449.
- 484 [18] S. GOTTLIEB, C.-W. SHU, AND E. TADMOR, *Strong stability-preserving high-order time dis-*  
485 *cretization methods*, SIAM Review, 43 (2001), pp. 89–112.
- 486 [19] M. HOCHBRUCK AND A. OSTERMANN, *Exponential integrators*, Acta Numerica, 19 (2010),  
487 pp. 209–286.
- 488 [20] H. J. HOGBEN, M. KRZYSTYNIAK, G. T. CHARNOCK, P. J. HORE, AND I. KUPROV, *Spinach—a*  
489 *software library for simulation of spin dynamics in large spin systems*, Journal of Magnetic  
490 Resonance, 208 (2011), pp. 179–194.
- 491 [21] J. HU AND R. SHU, *A second-order asymptotic-preserving and positivity-preserving exponential*  
492 *Runge–Kutta method for a class of stiff kinetic equations*, Multiscale Modeling & Simula-  
493 tion, 17 (2019), pp. 1123–1146.
- 494 [22] J. HUANG AND C.-W. SHU, *A second-order asymptotic-preserving and positivity-preserving dis-*  
495 *continuous Galerkin scheme for the Kerr–Debye model*, Mathematical Models and Meth-  
496 ods in Applied Sciences, 27 (2017), pp. 549–579.
- 497 [23] J. HUANG AND C.-W. SHU, *Bound-preserving modified exponential Runge–Kutta discontinu-*  
498 *ous Galerkin methods for scalar hyperbolic equations with stiff source terms*, Journal of  
499 Computational Physics, 361 (2018), pp. 111–135.
- 500 [24] L. ISHERWOOD, Z. J. GRANT, AND S. GOTTLIEB, *Strong stability preserving integrating factor*  
501 *Runge–Kutta methods*, SIAM Journal on Numerical Analysis, 56 (2018), pp. 3276–3307.
- 502 [25] L. JU, X. LI, Z. QIAO, AND J. YANG, *Maximum bound principle preserving integrating fac-*  
503 *tor Runge–Kutta methods for semilinear parabolic equations*, Journal of Computational  
504 Physics, 439 (2021), p. 110405.
- 505 [26] H. LI, S. XIE, AND X. ZHANG, *A high order accurate bound-preserving compact finite difference*  
506 *scheme for scalar convection diffusion equations*, SIAM Journal on Numerical Analysis,  
507 56 (2018), pp. 3308–3345.
- 508 [27] H. LI AND X. ZHANG, *On the monotonicity and discrete maximum principle of the finite*  
509 *difference implementation of  $C^0$ - $Q^2$  finite element method*, Numerische Mathematik, 145  
510 (2020), pp. 437–472.
- 511 [28] C. MOLER AND C. VAN LOAN, *Nineteen dubious ways to compute the exponential of a matrix,*  
512 *twenty-five years later*, SIAM review, 45 (2003), pp. 3–49.
- 513 [29] Z. SUN, J. A. CARRILLO, AND C.-W. SHU, *A discontinuous Galerkin method for nonlinear par-*  
514 *abolic equations and gradient flow problems with interaction potentials*, Journal of Com-  
515 putational Physics, 352 (2018), pp. 76–104.
- 516 [30] C. VILLANI, *Topics in Optimal Transportation*, vol. 58, American Mathematical Soc., 2021.
- 517 [31] F. YAN, J. VAN DER VEGT, Y. XIA, AND Y. XU, *Entropy dissipative higher order accurate posi-*  
518 *tivity preserving time-implicit discretizations for nonlinear degenerate parabolic equations*,  
519 Journal of Computational and Applied Mathematics, 441 (2024), p. 115674.
- 520 [32] X. ZHANG AND C.-W. SHU, *On maximum-principle-satisfying high order schemes for scalar*  
521 *conservation laws*, Journal of Computational Physics, 229 (2010), pp. 3091–3120.